Absolute Frequency of the $^{88}Sr^{+}$, 5s $^{2}S_{1/2}$- 4d $^{2}D_{5/2}$ Reference Transition at 445 THz and Evaluation of Systematic Shifts

A.A. Madej, J.E. Bernard, P. Dubé, and L. Marmet
Frequency and Time Group, Institute for National Measurement Standards
National Research Council of Canada, Ottawa, K1A 0R6, Canada

R.S. Windeler
OFS, 700 Mountain Ave., Murray Hill, New Jersey 070974 USA

PACS Numbers: 32.30.Jc, 32.80.Pj, 06.20.Fn, 06.30.Ft

Abstract: A Cs referenced optical frequency comb system has been used to measure the center frequency of the 5s $^{2}S_{1/2}$ – 4d $^{2}D_{5/2}$ transition at 445 THz in a single, trapped and laser cooled $^{88}Sr^{+}$ ion. The transition frequency ν_{SD} = 444 779 044 095 510 Hz ± 50 Hz (1σ) is obtained, when corrected for systematic shifts. A detailed calculation of the estimated systematic shifts is presented which yields improved values for the various shift parameters including blackbody and electric quadrupole moment shifts.

I. INTRODUCTION

The role of atomic frequency standards has been critical in the precision probing of physical theories and effects. Besides forming the basis for the units of physical measurement of time and length, these systems have been employed in the measurement of fundamental constants and subtle physical phenomena [1-3]. For many years, the most accurate realizations of frequency have been achieved using RF sources stabilized on hyperfine transitions in atoms [1]. The rapid development of ultra-high resolution optical spectroscopy and frequency comb technology have recently set the stage for optical clocks based on high Q transitions in atoms and molecules [1,4]. One of the approaches being studied is that of a single atomic ion suspended in a time varying trapping field and laser cooled to low temperatures [5]. These systems closely approach the ideal situation of an isolated quantum absorber at rest and have extremely low systematic perturbations. Significant progress has been obtained on ultra-narrow dipole forbidden reference frequencies in Ba^{+}, Sr^{+}, In^{+}, Yb^{+} and Hg^{+} [5-10]. To date, the best spectral resolution has been obtained for the Hg^{+} system for which a linewidth of 6.8 Hz has been observed and the transition frequency of 1065 THz has been measured to an accuracy of 10 Hz [10].

The $^{88}Sr^{+}$ system (figure 1) shows promise as a frequency standard. The $^{88}Sr^{+}$ ion has a simple energy level scheme [11] that matches with easily available laser technology, and has excellent potential accuracy and low systematic shifts [6]. Partially for these reasons, it was the first single ion system selected by the Comité International des Poids et Mesures (CIPM) as a reference for optical frequency [2]. The primary laser cooling and fluorescence excitation source at 422 nm can be obtained using a frequency doubled diode laser [12]. More recently, diode laser sources have become commercially available at this wavelength. Radiation at 1092 nm, available from either a diode-pumped fiber laser or a custom-made diode laser, is required to prevent optical pumping into the long-lived $^{2}D_{3/2}$ level (see fig.1). The “clock” transition of interest is the electric quadrupole, 5s $^{2}S_{1/2}$ – 4d $^{2}D_{5/2}$ transition at 445 THz (674 nm) which has a natural linewidth of 0.4 Hz [11]. This transition frequency is readily accessible using diode laser sources. In addition, the reference transition lies at a frequency with good overlap with existing frequency combs.

In contrast to other ion systems being investigated, the $^{88}Sr^{+}$ single ion reference transition has a linear Zeeman sensitivity to the ambient magnetic field. This frequency shift is not a significant limitation for the trapped ion reference. Magnetic shielding is necessary, but since the ion is localized to better than 0.1 μm^{3}, corresponding to the conditions for Doppler free spectroscopy (Lamb -Dicke regime), the problems of controlling the magnetic field and gradients over large volumes is alleviated. By measuring Zeeman components, which are symmetrically located about the line center, cancellation of the linear shift is directly obtained [6]. If the applied magnetic field is static and sufficiently temporally stable, it is possible to have a system giving high accuracy with small offset.

The Sr^+ system has been studied by a number of groups and examined as a frequency standard by the National Research Council of Canada (NRC) and the National Physical Laboratory in the U.K. (NPL) [5-7,11-14]. At NRC, early measurements of the absolute transition frequency yielding kilohertz-level accuracies were performed by heterodyning the 674-nm probe laser with radiation generated by frequency mixing a well-known laser standard at 633 nm and a frequency-chain-measured 10-µm laser source [14]. In 1998, the first direct absolute frequency measurement of a single ion transition in the visible region was performed using the NRC frequency chain yielding an accuracy of 200 Hz at 445 THz [6]. At the NPL, absolute measurements were initially obtained to an accuracy of 60 kHz using precision interferometry [13]. Recently, the group has used femtosecond laser based optical frequency combs to measure the single ion center frequency to ± 100 Hz [7]. They have also examined systematic effects by comparing different trap systems and have obtained a mean frequency difference of 34 ± 33 Hz in the two ion systems [15].

This paper describes recent optical frequency comb measurements at NRC of the Sr^+ S-D transition frequency using a femtosecond laser based system. Updated calculated systematic shift parameters and evaluations of the shifts for the current experimental apparatus are presented. The results indicate such shifts are small compared to the current measurement uncertainty and the ion system has potential for increased accuracy and reproducibility.

II. SINGLE ION REFERENCE STANDARD AND OPTICAL FREQUENCY MEASUREMENT SYSTEM

A more complete description of the single ion trap and the associated laser systems for cooling, detection, and probing has been given in previous work [6,12,16,17,18]. Briefly, a single ion of $^{88}Sr^+$ is confined in an electrodynamic quadrupole Paul type trap [5]. The trap has an endcap to center distance of z_o = 0.5 mm with a center to ring electrode distance of $r_o = (2)^{1/2} \times z_o$ = 0.71 mm. The trap electrodes are made of tantalum and have a spherical form for the endcap surfaces and semi-circular cross section for the ring electrode. A trapping voltage of 256 V amplitude is applied between the endcap and ring electrodes at a frequency of 12.0 MHz, providing a time averaged three-dimensional potential well of 10 eV depth. Based on measurements of the ion motion sideband spectra, the secular frequencies of the trap were measured to be ν_x = 940 kHz, ν_y = 980 kHz, and ν_z = 1990 kHz corresponding, respectively, to the two canonical radial oscillations and the axial oscillation frequencies. The ion is loaded using a single thermal source that produces an effusive beam of neutral Sr and electrons. Ionization can be controlled with low deposition rates of material on the electrode structure [19]. The micromotion due to trap imperfections and deposit related patch potentials are nulled by applying a dc bias through differential voltages between the axial endcap electrodes and a voltage difference between the nearby loading oven and the ring electrode. Detection of the micromotion amplitude is achieved by measuring the correlation between the rf drive and the fluorescence photon arrival time [5]. In this way, the micromotion is nulled along the beam probing direction, which has a projection along all three canonical trap vibrational axes. In the current experiment, the excitation beam is sent between the endcap and ring electrodes at an angle offset of 42° from the endcap axis direction.

A frequency-doubled diode laser system is used for laser cooling and fluorescence detection of the $5s\ ^2S_{1/2} - 5p\ ^2P_{1/2}$ resonance line at 422 nm. The laser is frequency stabilized in the long term via servo stabilization to a rubidium Doppler broadened absorption resonance [12] and is detuned several MHz below the 422-nm line center for effective Doppler laser cooling. The short-term linewidth of the laser is approximately 0.7 MHz over averaging times of 1 s and the Rb stabilization system controls the drift within a region of a few megahertz, which is well within the 22 MHz (FWHM) linewidth of the S-P transition. An output power of 60 µW at 422nm is focused to a spot size of ω = 15 µm at the ion location which is sufficient to ensure saturation of the excitation. A diode-pumped, multimode Nd: fiber laser at 1092 nm is used to ensure excitation on the $4d\ ^2D_{3/2} - 5p\ ^2P_{1/2}$ transition such that the ion does not relax into the long lived $^2D_{3/2}$ metastable level. . After exiting the laser, the light is passed through a 15 -MHz electro-optic modulator, which rapidly modulates the polarization of the 1092 nm light. In this way, optical pumping into specific Zeeman sub-levels of the $^2D_{3/2}$ state is avoided at small levels of background B field. The linewidth of the laser is 2 GHz with a power of 110 µW focused to a spot size of 60 µm. The 1092nm laser is maintained in resonance with infrequent manual tuning of the

laser during the experiment. The 422nm resonance fluorescence is collected using f/2 optics and imaged onto a 0.3 mm diameter aperture, which allows the signal light to enter a photon counting photomultiplier system. Single ion fluorescence rates of 6000 counts/s were observed in this work with background scattered light levels of less than 200 counts/s.

Probing on the narrow 0.4 Hz natural linewidth 5s $^2S_{1/2}$ – 4d $^2D_{5/2}$ transition is obtained using a frequency stabilized 674 nm diode laser system. In contrast to previous work [18], the master diode laser was an external cavity diode laser system with a Littman cavity configuration. The short-term linewidth of the diode laser was approximately 300 kHz in a 0.1 s averaging time. This laser oscillator linewidth was broader than that obtained with a previous system, which used external optical feedback from a Fabry-Perot resonator, but yielded much more reliable operation at the required frequency. The laser was stabilized using Pound-Drever-Hall stabilization [5] to an evacuated and thermally stabilized cavity made of ultra-low expansion glass (ULE) having a finesse of 15000 at 674 nm. Details concerning the layout and vibration isolation of the system are given in reference [18]. The frequency stabilized output of the probe laser was frequency shifted into resonance with the Sr^+ transition frequency with a double pass through an acousto-optic modulator giving a total frequency shift of approximately 410 MHz. Approximately 200 μW of the unshifted 674-nm probe laser light was sent via optical fiber to the laboratory housing the optical frequency comb apparatus. Up to 5 μW of 674 nm light was available to be focused on the single ion using a spot size of 30 μm. Typically, light powers of 10 to 200 nW were incident on the ion in order to prevent power broadening of the S-D transition. The laser linewidths encountered in the present work were in the range of 0.4 to 1 kHz depending on laser servo parameters. Typical drift rates of 900 Hz/day were observed due to long term changes in the reference ULE cavity length. However, shorter-term drifts of the laser stabilized to the cavity were observed to be much greater, typically being 4 kHz/hr. The origin of this drift has been determined to be due to spurious reflections in the fiber coupling to the ULE cavity causing variations in the lock point for the Pound-Drever-Hall stabilization [18]. The linewidth used in the current work was inferior to that obtained with our previous system, which employed optical feedback narrowing. Nevertheless, as will be seen, reproducibilities at the tens of Hertz level could be obtained with the current probe system. A new probe laser system has been recently developed which now provides a linewidth of 100 Hz or better [20] but this system was not available at the time of the current reported measurements.

Excitation of the S-D transition by the 674-nm probe causes shelving to the upper 4d $^2D_{5/2}$ metastable state, which can be detected through quantum jumps in the 422-nm fluorescence [11]. In this way, detection of nearly every 674 nm transition event is achieved. A bias magnetic field of typically 14 μT was used to split the S-D transition into 10 well-separated Zeeman components. The field was generated using a pair of coils in Helmholtz configuration aligned along the probe beam propagation direction and driven with an ultra-low noise current supply (ILX-3620). A single layer magnetic shield (CO-NETIC AA) reduced the effects of slowly varying dc magnetic fields and strongly shielded against ac field broadening and shifts. As will be seen, such perturbations appear to be below the Hertz level in the current experiment.

The frequency of the probe laser system was referenced to two Zeeman components by servo stabilizing the AOM shifted radiation using the technique described in [17] and recording the applied AOM shift frequency simultaneously with the frequency comb measurements of the unshifted probe laser light. In this work, measurements were performed using the innermost $(m_{J''}, m_{J'}) = (\pm 1/2, \pm 1/2)$ components having a Zeeman splitting of ± 78 kHz or the next symmetrically located $(m_{J''}, m_{J'}) = (\pm 1/2, \pm 3/2)$ components having a relative splitting of ± 156 kHz from line center. No discernable relative frequency shift in the line center was observed when using either set of components. Also, frequency lock studies were made at different applied bias magnetic fields with no observed change in the determined frequency. The typical cycle time for the servo lock was 20 s for probing at the four half intensity points on the two Zeeman components.

The optical comb and the system for measuring the frequency of the 674 nm probe laser are shown in Fig. 2. The comb used in this work is of conventional design [21-23] and has been described elsewhere [16,24]. A mode-locked Ti:sapphire laser (GigaOptics Gigajet 20), pumped by 5 to 6 W at 532 nm (Coherent Verdi V-8), produces a regular train of 30 to 50-fs pulses at a

repetition rate of approximately 700 MHz. The output is focused into a 20 to 30-cm-long piece of microstructured fiber [25] in which the spectrum is broadened to over an octave from approximately 500 nm to 1100 nm. The spectrum consists of a regular comb of optical frequencies separated by the pulse repetition frequency, f_{rep} and has an extrapolated offset frequency from 0 Hz of f_o. A servo with an open-loop unity-gain frequency of 2 kHz is used to phase lock the repetition frequency to a high quality synthesizer (Agilent 4423B) through piezo control of the laser cavity length. The synthesizer is referenced to a 10-MHz signal provided by one of the NRC hydrogen masers, which in turn is monitored through the NRC cesium clock ensemble. The uncertainty of the reference 10-MHz signal from International Atomic Time (TAI) was better than 2×10^{-14}. Measurements were made in the same gravity potential as the time standards. A self-referencing system [22], which uses a 5-mm-long KTP doubling crystal, is used to measure f_o. The f_o heterodyne signal is amplified and filtered before being digitally divided by 80 or 256 and phase locked, through pump-power modulation of the femtosecond laser. The divided signal is phase locked to the output from a second maser-referenced synthesizer (SRS DS345) (servo open-loop unity-gain frequency of 70 kHz). The comb of optical frequencies from 500 nm to 950 nm is combined on a beam splitter with the 674 nm light from the probe laser system. A 1200-line/mm grating is used to reflect the spectral region of interest onto an avalanche photodiode, which detects the heterodyne beat frequencies, f_B, between the light from the 674 nm laser and the nearest comb elements. A bandpass filter is used to select one of these beat frequencies for counting. Typical beat frequency signal-to-noise ratios of the unshifted probe and the nearest comb element were approximately 35 dB in a 100 kHz bandwidth.

III. RESULTS

An example of the observed lineshape for the $(m_{J''}, m_{J'}) = (-1/2, -1/2)$ Zeeman component is given in Fig. 3. The fitted linewidth, using a Lorentzian form, was 410 Hz ± 50 Hz. The magnitude of the spectral shift sensitivity of a Zeeman component to a change in magnetic field is proportional to the relative distance from line center. A plot of the linewidth versus the relative Zeeman shift sensitivity is shown in Fig. 4 for four different components. The results confirm that there is little perturbation of the lineshape by ac magnetic fields since components with different sensitivities to the background field exhibit the same linewidth. A more complete discussion of the systematic shift sensitivity is given in Section IV.

Determination of the absolute frequency of the S-D line center was obtained in two parts. The probe laser frequency was determined by averaging sets of the 1-s comb frequency readings of the laser stabilized to the ULE cavity. These values were combined with the results of the AOM-shift needed to maintain the radiation at the ion transition line center. The required AOM shift frequencies were updated with a cycle time of approximately 20 s. Figure 5a shows the results of a series of 1-s comb measurements of the frequency of the 445-THz probe laser. Figure 5b shows the corresponding 20-s frequency offset values determined by the servo system steering the AOM-shifted frequency into resonance with the ion transition. As can be seen, the fluctuations in the laser frequency are followed in the AOM lock to the ion. Drifts in the probe laser frequency result in a lag in the lock of the AOM-shifted laser frequency to the S-D line center. The resulting offset of the AOM lock can be calculated from the measured drift rate and knowledge of the Zeeman component linewidth and the AOM-lock servo gain [17]. With such corrections, the observed S-D center frequency was determined for each 20-s average and is shown in Figure 5c. As can be seen, the line center determinations show a symmetric distribution centered on the mean value.

Figure 6 shows the Allan deviation of the 1-s measurements of the probe laser frequency for the run shown in Fig. 5. The Allan deviation improves from 700 Hz for an averaging time of 1 s to just over 100 Hz at 10 s averaging time. At longer times, the drift of the probe laser becomes apparent and thus the stability does not improve with further averaging time. In some runs, the drift was even more pronounced and the Allan deviation increased significantly for longer averaging times. Figure 6 also shows the instability of the 20-s determinations of the line center frequency shown in Fig. 5c. This value improves with averaging time from 150 Hz at 20 s down to about 20 Hz at 500 s. The instability floor for the frequency determinations varied as a function of the drift of the probe laser frequency indicating that the AOM servo stabilization to the ion suffered increased uncertainty for some runs depending on the probe laser performance. The line

center frequency for each run was obtained using a weighted mean of approximately 40 to 80, 20-s readings with the uncertainty based upon the stability floor observed for each run. The primary limitation on measurement times was due mostly to the probe laser unlocking from the ion resonance due to drift of the laser lock to the ULE reference cavity. A summary of absolute frequency results for each run on the four experimental days is shown in Fig. 7. The measurements were performed over a time period spanning August 2002 to November 2002. Large error bars correspond to periods of high drift in the probe laser resulting in relatively poorer stability of the lock value. Based on the results, an average center frequency of the ion transition of ν_{SD} = 444 779 044 095 495 ± 50 Hz (1σ) is obtained. The result is in agreement with our previous chain-based measurement of 444 779 044 095 400 ± 200 Hz [6] and also agrees with the value of ν_{SD} = 444 779 044 095 520 ± 100 Hz (1σ) by Margolis et al. [7]. The present series of measurements appears to be limited by the current probe laser linewidth and drift. Recent work has been directed toward the construction of a two-stage high finesse cavity stabilized probe laser, which has far less drift and possess improved linewidth [20].

IV. DISCUSSION

A. Systematic effects on the single ion system and determinations of parameter sensitivities

One of the key advantages in the use of a single trapped and laser cooled ion in the probing of ultra-narrow transitions is the high level of immunity of these systems to external perturbations. An important part of the determination of the center frequency of the reference transition and its utilization as an optical frequency standard is the evaluation of such sensitivities. In this work, we present a comprehensive listing of causes of spectral shifts together with calculations of the various sensitivity parameters for the $^{88}Sr^{+}$ system.

B. Second order Doppler shift

The motion of the ion caused by its thermal kinetic energy and the driven motion caused by the applied RF trapping field can shift the position of the line center due to the relativistic time–dilation [5]. This time dilation shift, also known as the second-order Doppler shift, is produced by the ion moving relative to the laboratory frame. In order to obtain values for this effect for the current experiment, studies of the intensity of secular and micromotion sidebands were obtained for the operating conditions used in the frequency measurements. The relation between the first order secular sideband intensity to that of the carrier has been shown to be [26]:

$$\left[\frac{\sigma(1)}{\sigma(0)}\right] \cong \left(1+\frac{h\nu_m}{2k_BT}\right)\times\frac{I_1(u)}{I_0(u)} \qquad (1)$$

where $u = \frac{k_m^2 h}{4\pi^2 M \nu_m}\left(\frac{k_B T}{h\nu_m}-\frac{1}{2}\right)$ (2)

here k_B is Boltzman's constant, h is Planck's constant, ν_m is the secular frequency of the ion motion in the m'th direction, M is the mass of the atom and k_m is the projection of the wavevector, $k = 2\pi/\lambda$ on the direction of motion. The function $I_n(u)$, is the modified Bessel function of order n. Based on a series of measurements taken along different canonical motion directions, a mean kinetic temperature was determined to be T = 38 mK ± 10 mK, which is higher than previously observed [6]. The higher secular motion temperature may be due to the use of the 422 nm cooling radiation near peak intensity in order to maximize ion fluorescence.

The second order Doppler shift can be estimated via the relation [27]:

$$\left(\frac{\Delta\nu_{D2}}{\nu}\right)_{therm} = \frac{-3k_B T}{2Mc^2} \tag{3}$$

Using the observed ion kinetic temperatures, the thermal contribution to the shift in the center frequency is estimated to be (-0.027 ± 0.007) Hz or (-6.0 ± 1.6) × 10^{-17}.

Although the micromotion-induced sidebands at ± 12 MHz were observed to be small, such motion was the main contribution to the second order Doppler shift. Based on the relations presented by Berkeland and coworkers [27], the contribution to the second order Doppler effect due to micromotion is related to the micromotion sideband intensity via:

$$\left(\frac{\Delta\nu_{D2}}{\nu}\right)_{micro} \approx -\left(\frac{\Omega}{ck\cos\phi}\right)^2 \frac{\sigma(1)}{\sigma(0)} \tag{4}$$

where $\Omega = 2\pi \times 12$ MHz is the angular frequency of the trap field, k is the wavevector of the probe field, ϕ is the angle between the observation direction and the direction of micromotion, and $\sigma(1)/\sigma(0)$ is the ratio of the 1st observed sideband intensity to the carrier line. Results from these studies give a contribution due to micromotion of (-0.16 ± 0.10) Hz, (-3.6 × 10^{-16} ± 2.2 × 10^{-16}). The current experimental apparatus allows the probing of only one direction within the trap. This direction has a projection on all the principal canonical directions of the trap and thus should be able to sense any imbalances in micromotion between different canonical directions. It is unlikely that the nulling of micromotion performed in the loading and preparation process nulled the micromotion in the probe direction but left a higher residual level in the other orthogonal directions. In order to see if there was any significant perturbation to the ion center frequency due to this possibility, studies were performed in which a deliberate variation in the micromotion was introduced via a change of the axial trim voltage. This lead to micromotion levels over an order of magnitude higher than when the trim voltage was optimally adjusted. The results are plotted in Fig. 8. Here the measured relative frequency of the S-D center is shown based on the probe laser lock to the ion. Despite the large amount of micromotion being applied to the ion, no observed variation on the ion center frequency was detected at a level of 10 Hz. This result supports the view that the micromotion contributions to the systematic shifts are not a limitation at the present accuracy of the ion center frequency.

B. Stark effects

The Stark shifts of the 5s $^2S_{1/2}$ and the 4d $^2D_{5/2}$ levels play a significant role in the overall systematic shift uncertainties for the current experimental setup. The sources for such shifts arise from a number of factors. The background blackbody radiation from the trap and surrounding environment causes a time averaged isotropic ac Stark shift of the energy levels. Moreover the micromotion and thermal secular motion displaces the ion from the ideal null point at the center of the trap and thus causes shifts. Finally, the radiation used to probe the ion reference transition at 674 nm and the radiation from an auxiliary repumping source at 1092 nm cause shifts of the energy levels via the ac Stark effect. The following section serves to quantify some of these effects for the present experimental arrangement.

1.Estimate of Stark shift coefficients

In order to obtain accurate estimates for the magnitude of the shift, it is important to determine the scalar polarizability of the 5s $^2S_{1/2}$ level and the scalar and tensor polarizability of the 4d $^2D_{5/2}$ level [28]. The calculations that follow are based on oscillator strength data drawn from three sources. Gallagher [29] obtained lifetime and oscillator strength data for the low-lying Sr^+ levels through measurements of the Hanle Effect. More recently, calculations by Brage et al. of several oscillator strengths were obtained using ab-initio multiconfiguration Hartree-Fock calculations of the wavefunctions [30]. There also exist extensive tabulations of the Ca^+ ion levels [31]. By scaling the lower level Ca^+ oscillator strengths to match those known for Sr^+, a reasonable

estimate of the magnitude of the oscillator strengths for higher lying levels of Sr^+ were obtained. A tabulation of the results obtained for these various sources is given in Table I. Using the relations presented by Khadjavi et al. [28], we have for the scalar (α_0) and tensor (α_2) polarizabilities:

$$\alpha_o = -\frac{8\pi\varepsilon_o\ K_o}{\left[3(2J+1)\right]^{1/2}} \tag{5}$$

and

$$\alpha_2 = 16\pi\varepsilon_o\ K_2\sqrt{\frac{5}{6}}\left[\frac{J(2J-1)}{(2J+3)(2J+1)(J+1)}\right]^{1/2} \tag{6}$$

where

$$K_L = \frac{3\,(2J+1)\,r_o}{8\pi^2}\sum_{J'}(\lambda_{JJ'})^2\ \ f_{J'J}\begin{Bmatrix} J & J & L \\ 1 & 1 & J' \end{Bmatrix}(-1)^{J+J'} \tag{7}$$

where ε_o is the permittivity of free space, r_o is the classical electron radius, J is the state angular momentum, L = 0 , 2, $\lambda_{JJ'}$ is the transition wavelength and $f_{J'J}$ is the oscillator strength where $f_{J'J}$ is positive if the J' state lies higher than the J state. For the $^2S_{1/2}$ level, the scalar polarizability is the only term present. Employing the data from Gallagher gives a value of $\alpha_0 = 1.419 \times 10^{-39}$ C^2 s^2 kg^{-1}, while using the Brage et al. values, one obtains $\alpha_o = 1.391 \times 10^{-39}$ C^2 s^2 kg^{-1}. Recently Warrington has performed a similar compilation of transition strength data from other sources [32]. Based on four different sources of transition strengths, he has obtained values of α_o ranging from 1.35×10^{-39} to 1.49×10^{-39} C^2 s^2 kg^{-1}. Based on these series of calculations one may estimate the current confidence in $\alpha_o(^2S_{1/2})$ to be $\pm 0.06 \times 10^{-39}$ C^2 s^2 kg^{-1}. Thus we may assign: $\alpha_o(^2S_{1/2}) = (1.40 \pm 0.06) \times 10^{-39}$ C^2 s^2 kg^{-1}.

For the 4d $^2D_{5/2}$ level, the biggest terms that contribute are the nearby 5p $^2P_{3/2}$ state and the 4f $^2F_{5/2}$ state. Using the oscillator strength data by Brage et al. [30] we obtain $\alpha_o = 7.4 \times 10^{-40}$ C^2 s^2 kg^{-1} and $\alpha_2 = -6.7 \times 10^{-40}$ C^2 s^2 kg^{-1} for the scalar and tensor contributions, respectively. Repeating the calculation using the scaled Ca^+ oscillator strengths [31] yields $\alpha_o = 1.0 \times 10^{-39}$ C^2 s^2 kg^{-1} and $\alpha_2 = -8.7 \times 10^{-40}$ C^2 s^2 kg^{-1}. Warrington has reported that from the four sets of alternate data, results of $\alpha_o(4d\ ^2D_{5/2})$ ranging from 5.9×10^{-40} to 9.2×10^{-40} C^2 s^2 kg^{-1} were obtained [32]. We thus employ: $\alpha_o(4d\ ^2D_{5/2}) = (8 \pm 2) \times 10^{-40}$ C^2 s^2 kg^{-1} and $\alpha_2(4d\ ^2D_{5/2}) = (-7 \pm 2) \times 10^{-40}$ C^2 s^2 kg^{-1} as our current estimates of the polarizabilities of the upper state.

For the general case of the perturbing electric field whose field direction makes an angle θ with respect to the quantization axis of the atom, the Stark shift of an individual level can be expressed as [33]:

$$\Delta\nu_S = \frac{1}{h}E^2\left\{-\frac{1}{2}\alpha_o - \frac{1}{4}\alpha_2\left(3\cos^2\theta - 1\right)\frac{\left[3m^2 - J(J+1)\right]}{J(2J-1)}\right\} \tag{8}$$

where E is the magnitude of the electric field. For the 5s $^2S_{1/2}$ level there is no tensor polarizability and thus there is no angle dependence. A shift rate for the $m_J = \pm 1/2$ levels of the ground state is thus estimated as $\gamma_S = \partial\nu/\partial E^2 = (-1.06 \pm 0.04)$ $\mu Hz/(V/m)^2$. Similarly the scalar contribution to the shift of the $^2D_{5/2}$ level would yield a shift of (-0.6 ± 0.2) $\mu Hz/(V/m)^2$. The total shift of the upper level is in general dependent on both the m_J level and the angular orientation of the field relative to the quantization axis.

2. Blackbody radiation shift

Given that the thermal background field is isotropic, the tensor contribution to the Stark shift averages to zero and the scalar contributions are those that remain significant. For the blackbody spectrum at room temperature, the frequencies of the perturbing field are greater than the natural linewidth but much less than the atomic transition interval. For this case, the system can no longer follow the variation of the electric field but responds only to the time average rms electric field [34]. Hence the mean blackbody shift can be written as:

$$\Delta\nu_{BB} = -\frac{1}{2h}\left\langle E^2(t)\right\rangle(\alpha'_o - \alpha_o) \tag{9}$$

where $\langle E^2(t)\rangle$ is the time averaged quadratic electric field strength of the black body radiation, and α'_o and α_o are the scalar state polarizabilities in the excited and ground state, respectively. For a given background temperature T, the value of $\langle E^2(t)\rangle$ is given by [34,35] :

$$\left\langle E^2(t)\right\rangle = (832\ \text{V/m})^2 (T/300\ \text{K})^4 \tag{10}$$

For a room temperature background (T=293 K) this would thus correspond to a shift of $\Delta\nu_{BB}$ = (+0.30 ± 0.11) Hz. Recently, Warrington has performed detailed calculations using more exact calculations incorporating the blackbody frequency dependence [32]. The results obtained for his various data sources yield blackbody shifts ranging from 0.249 Hz to 0.469 Hz, which are in good agreement with our estimated value.

3. Stark Shifts due to micromotion and thermal motion

The driven motion and the thermal secular motion of the ion in the trap cause the ion to be exposed to electric fields from the trap field that have non-zero time averaged values. From Berkeland et al. [27], the Stark shift created by micromotion is given approximately by:

$$\left(\Delta\nu_S\right)_{micro} \cong 2\,\gamma_s\left(\frac{2\,M\,\Omega^2}{qk\cos\phi}\right)^2 \frac{\sigma(1)}{\sigma(0)} \tag{11}$$

where $\gamma_S = \partial\nu/\partial E^2$ is the Stark shift rate, Ω is the trap angular frequency, M is the mass of the ion and q its charge, k is the wavevector of the probe light and ϕ the angle between the micromotion direction and the incident light. Using our previously obtained ratio of sideband intensities and estimates of the projection of the probe beam wavevector on the micromotion direction, micromotion induced Stark shifts of $(\Delta\nu_S)_{micro}$ =(0.9 ± 0.9)Hz for the $(m_{J''}, m_{J'})$ = (±1/2, ±1/2) transitions and $(\Delta\nu_S)_{micro}$ = (0.7 ± 0.7) Hz for the $(m_{J''}, m_{J'})$ = (±1/2, ±3/2) are estimated. The dominant source in the uncertainty is in the determination of the angular projection of the micromotion on the probe beam direction.

For the thermal secular motion contribution to the Stark shift, the frequency shift can be expressed as:

$$\left(\Delta\nu_S\right)_{therm} \approx \gamma_s\,\frac{3M\Omega^2 k_B T}{q^2} \tag{12}$$

Using our estimated ion kinetic temperature based on sideband measurements, thermally induced Stark shifts of $(\Delta\nu_S)_{therm}$= (36 ± 18) mHz are estimated for the (±1/2, ±1/2) components while a shift of $(\Delta\nu_S)_{therm}$= (29 ± 12) mHz is estimated for the (±1/2, ±3/2) component pair. It can be seen that the thermal contribution is nearly two orders of magnitude smaller than the contribution from micromotion. In future experiments, a higher degree of control of micromotion will be needed to ensure that this systematic frequency shift does not dominate.

4. AC Stark shift

The rapidly oscillating fields of the optical radiation incident on the ion during the probe cycle can perturb and shift the line center of the ion transition. In the present arrangement, both the 674 nm (445 THz) probe and the1092 nm $^2P_{1/2}$-$^2D_{3/2}$ repumping radiation are present during the interrogation cycle. As pointed out by Margolis et al. [7], this contribution to the Stark shifts may

be significant. The mean frequency shift of an energy level of state "s" subject to radiation at angular frequency ω and electric field amplitude $\mathbf{E}_o$ has been given as [37];

$$\left(\Delta\nu_S\right)_{AC} = \frac{\pi}{h^2}\sum_{s\neq n}\overline{\left|\langle n\,|\,\mathbf{E}_o\bullet\mathbf{p}\,|\,s\rangle\right|^2}\;\frac{\omega_{ns}}{\omega_{ns}^2-\omega^2} \tag{13}$$

where ω_{ns} is the angular transition frequency and the time average of the square magnitude of the dipole matrix element is taken. Following a derivation similar to that provided by Khadjavi et al. [28] for the static field case, the above expression can be written as equivalent to a first order perturbation. Expanding the effective AC Stark Hamiltonian in terms of spherical basis notation, a solution to the ac Stark shift can be written as:

$$\left(\Delta\nu_S\right)_{AC} = \frac{8\pi\, I_o}{hc}\left\{-\tfrac{1}{2}\beta_o - \tfrac{1}{4}\,\beta_2\left(3\cos^2\theta-1\right)\frac{3m^2-J(J+1)}{J(2J-1)}\right\} \tag{14}$$

where

$$\beta_o = -\frac{2U_o}{\left[3(2J+1)\right]^{1/2}} \tag{15}$$

and

$$\beta_2 = 4\,U_2\,\sqrt{\tfrac{5}{6}}\left[\frac{J(2J-1)}{(2J+3)(2J+1)(J+1)}\right]^{1/2} \tag{16}$$

and where

$$U_L = \frac{3\,(2J+1)\,c^2\,r_o}{16\pi^2}\sum_{J'}\frac{f_{JJ'}}{\left(\nu_{JJ'}^2-\nu^2\right)}\begin{Bmatrix} J & J & L\\ 1 & 1 & J'\end{Bmatrix}(-1)^{J+J'} \tag{17}$$

Here I_o is the intensity of the incident light of frequency ν, and θ is the angle between the polarization directions for the linear polarized light and the quantization axis. Using tabulations of the 6j symbols and the oscillator strengths listed in Table 1, the ac stark effect was calculated for our current experimental conditions. For both the 674nm light and the 1092 nm radiation, the polarization direction was orthogonal to the quantization direction since the bias magnetic field was applied along the incident beam direction. Thus θ = 90º in our arrangement. We can express the state shift as a function of the intensity by defining the parameter κ such that:

$$\left(\Delta\nu_S\right)_{AC} = \kappa\, I_o \tag{18}$$

Tabulations for the parameter κ for the S and D states under the condition of θ= 90º are presented in Tables 2 and 3 for perturbation by 674 nm and 1092 nm light respectively and are given in units of mHz/(W/m^2). The tabulations employ oscillator strength data from Brage et al. [30], the scaled Ca^+ strengths [31], and the experimental oscillator strengths of Gallagher [29]. The results show that the total transition shifts are comparable in magnitude for the two wavelengths with the $^2D_{5/2}$ level exhibiting a change of sign between the 674 nm and 1092nm results. It should also be noted that the relative order of Stark shift sensitivity of the D state components reverses when calculations for the shift at θ= 0º are determined.

In our current measurements, the powers incident on the ion were P_{674} = (0.20 ± 0.05) μW and P_{1092} = (105 ± 11) μW focused to a spot size of ω_o(674nm)= (30 ± 10) μm and ω_o(1092nm)= (60 ± 20) μm respectively. Using our intensity shift coefficients, one obtains that for our

conditions, we would expect a shift for the (±1/2, ±1/2) components of $\Delta\nu_S$ = +0.10 ± 0.06 Hz due to the 674 nm radiation and $\Delta\nu_S$ = (-12 ± 12) Hz due to the 1092 nm radiation. For the (±1/2, ±3/2) Zeeman component, the ac Stark shifts are $\Delta\nu_S$ = (+0.10 ± 0.06) Hz and $\Delta\nu_S$ = (-21 ± 21) Hz for the 674-nm and 1092-nm radiation, respectively. The presence of the 1092-nm radiation in the current series of measurements has a significant contribution to the determination of the unperturbed frequency value. Given the relatively strong systematic shift due to the presence of the 1092-nm radiation, future experiments will employ a probing cycle where the repumping beam is blocked during the 674 nm interrogations [38].

D. Electric quadrupole shift of the 4d $^2D_{5/2}$ level

The existence of a non-spherical charge distribution for the electron in the upper D level results in a quadrupole moment that can interact with the field gradient of any static or ac fields present in the trap. Since the shift is linear with the field gradient, rapidly oscillating harmonic fields, such as the rf trapping field, do not significantly shift the line center but effectively produce sidebands well away from the line center. The presence of static fields within the trap is of greater concern since patch potentials on the order of a volt may be present on the trap electrode structure and can create a sufficiently strong field gradient. Itano has presented a theoretical treatment for the quadrupole moment shift for an arbitrary angular orientation between a field gradient and the quantization axis [39]. We have performed calculations using hydrogenic wavefunctions [40] for the 4d $^2D_{5/2}$ level. By fitting the actual state energy to an effective hydrogenic energy level, with effective quantum number n^* = 2.43, a matrix element $\langle 4d|r^2 \mid 4d\rangle$ = 9.24 a_o^2 was obtained where a_o is the Bohr radius. A more accurate result provided by Itano [41] using atomic wavefunction computer calculations, first developed by Cowan [42], yields 10.59 a_o^2, in good agreement with the hydrogenic result. This result is indicative that the $^2D_{5/2}$ orbital does not strongly deviate from the single-electron result. Substituting the parameters for the Sr^+ 4d $^2D_{5/2}$ state into the relations presented by Itano gives for the $^2D_{5/2}$ level,

$$\left\langle 4d,\tfrac{5}{2},\tfrac{5}{2},m \mid H_Q \mid 4d,\tfrac{5}{2},\tfrac{5}{2},m\right\rangle = \left(\tfrac{1}{4}-\tfrac{3}{35}m^2\right) A\, q \left(3\cos^2\beta - 1\right)\left\langle 4d \mid r^2 \mid 4d\right\rangle \qquad (19)$$

where β is the angle between the field gradient direction and the quantization axis of the ion. Assuming a field gradient roughly along the axial direction of the trap would give $\beta \approx 40^o$. A value for the parameter $A \approx 50$ V/cm^2 is estimated based on the level of patch potentials thought to reside on electrodes and residual bias potential between the endcap and ring electrodes. For these values, a quadrupole shift of $\Delta\nu$ = +0.55 Hz for the (±1/2, ±1/2) components and $\Delta\nu$ = +0.14 Hz for (±1/2, ±3/2) transitions is estimated. These can be considered as an upper limit to the magnitude of the shift.

E. Zeeman effects

1.Linear Zeeman effect (ac broadening and shifts)

By probing on symmetric components, the dc linear Zeeman shift is effectively cancelled out in the current experimental measurements. However, AC fields penetrating through shielding may cause broadening and distortion of the line shape resulting in a shift of the line center. As was shown in Fig. 4, measurements of the linewidths of S-D components with different Zeeman sensitivity show no detectable change. By fitting the observed data, broadening of the innermost component is estimated to be below 27 Hz. Also, measurements of the shielding factor of the magnetic shield together with measurements of the external ac fields result in an estimated linewidth below 1.7 Hz. The temporal form of the ac field detected in the external lab environment is reasonably symmetric. Thus, the ac field contribution to the shift of the line center is considered to be below one tenth the estimated broadening or $\Delta\nu$ < 0.2 Hz.

2.Second order Zeeman Shift

The higher order contribution to the Zeeman effect has a quadratic component that shifts the frequencies of both symmetric S-D Zeeman components in the same direction and thus introduces a systematic shift in our line center determination. By using second order perturbation theory [40], these shifts have been determined to be:

$$\Delta\nu_{Z2} = \tfrac{6}{25}K;\ \ m = \pm\tfrac{1}{2}$$
$$\Delta\nu_{Z2} = \tfrac{4}{25}K;\quad m = \pm\tfrac{3}{2} \qquad (20)$$
$$\Delta\nu_{Z2} = 0\,;\quad m = \pm\tfrac{5}{2}$$

where

$$K = \frac{\mu_B^2\ B^2}{h^2\ \nu_{DD}} \qquad (21)$$

here μ_B is the Bohr magneton, B the ambient magnetic field, and ν_{DD} is the frequency separation of the metastable 4d $^2D_{3/2,5/2}$ fine structure levels. For $^{88}Sr^+$, $\nu_{DD} = 8.41 \times 10^{12}$ Hz, thus resulting in a relatively weak dependence on B field. The result gives $\Delta\nu_{Z2} = 5.6\ \mu Hz/\ \mu T^2$ for the (±1/2 ±1/2) components and 3.7 $\mu Hz/\ \mu T^2$ for the (±1/2, ±3/2) components. For our typical field intensities of (14 ± 2) μT, this leads to a shift of (+1.1 ± 0.2) mHz for the (±1/2, ±1/2) components and (+0.40 ± 0.06) mHz for the (±1/2, ±3/2) components. The blackbody radiation field also has a non-zero mean square magnitude of magnetic field, which can be expressed as [36]:

$$\left\langle B^2(t)\right\rangle = (2.8\,\mu\mathrm{T})^2\ (T/300\,\mathrm{K})^4. \qquad (22)$$

For a room temperature system at T=293 K, $\langle B^2(t)\rangle = 7.13\ \mu T^2$ and thus the estimated shifts on the (± ½, ± ½) components would be +40 μHz while for the (±1/2, ±3/2) components the shift would be +26 μHz. Clearly such contributions will be masked by the other perturbations at the current level of resolution and operating conditions.

F. Collisional shifts and broadening

Estimates of the broadening of the Zeeman components and the shift of the linecentre resulting from collisions with non-polar gas molecules can be obtained using a pure induced polarization model to calculate the classical (Langevin) collisional rate constant [43].

$$k = \langle \sigma\, \mathrm{v}\rangle = \frac{1}{2\varepsilon_o}\, q\left(\frac{\alpha}{\mu}\right)^{1/2} \qquad (23)$$

where q is the charge of the ion, α is the static polarizability of the perturbing gas atom/molecule, and μ is the reduced mass of the Sr^+ -gas perturber system. In the current experiment, the principal gas contaminant is H_2 whose partial pressure is an order of magnitude larger than that of other gas species. Using a calibrated quadrupole residual gas analyzer attached to the ion trap apparatus, the measured partial pressure of H_2 was found to be $P_{H2} = 7 \times 10^{-8}$ Pa . The calculated Langevin rate constant for $^{88}Sr^+$ with H_2 being the perturber is $< \sigma\, v >_{coll} = 1.5 \times 10^{-15}\ m^3\ s^{-1}$. This yields a collisional rate of $\gamma_{coll} = 0.03\ s^{-1}$ and an estimated broadening contribution of $\Delta\nu_{coll} = 8$ mHz. The magnitude of any line shift due to such effects would be expected to be smaller than the broadening.

Studies of the collision induced shift of the ^2D series lines in Rydberg-like alkali atoms have been performed [44]. The results indicated a line shift that scaled as $n_{eff}^{2.4}$ where n_{eff} is the effective quantum number. Using the self-broadening and shift results for Rb, the shift for the isoelectronic $^{88}Sr^+$ 4d $^2D_{5/2}$ level can be estimated. The values for Rb can then be scaled by the increase in the collisional rate due to polarization by the Sr^+ ion relative to the neutral Rb case. For the 4d $^2D_{5/2}$ level, the shift rate is thus estimated as: $\Delta\nu_{shift} = 1.0 \times 10^4$ Hz/Pa $(n_{eff})^{2.4}$.

Fitting the Sr^+ D series to a Rydberg line progression yields $n_{eff} = 2.42$ for the 4d $^2D_{5/2}$ level; thus the mean shift is estimated as: $\Delta\nu_{shift} = 8 \times 10^4$ Hz/Pa . Assuming the hydrogen gas perturber shift rate is on the same order as the broadening, then an estimate of the lineshift given our current

gas environment would be $\Delta\nu_{shift}$ = 5 mHz. It should be stressed that the above calculations are estimates and that more detailed studies would be beneficial to quantify such shifts more precisely. Nevertheless, the equivalence between the collisional broadening and shift, calculated using the Langevin classical rate, and the extrapolation, using the Rb Rydberg studies, confirms that such collision effects are indeed quite small and are unobservable at the current level of experimental precision. The collisional shift can be readily reduced through modifications to the experimental apparatus such as the use of titanium sublimation pumps and refrigerated cold surfaces, which would yield working pressures of 10^{-9} Pa or below.

G. Summary of shifts and correction of the S-D frequency

Table 4 summarizes the systematic shifts calculated for the current system. The total estimated correction is (–10 Hz ± 12) Hz for the (±1/2, ±1/2) components and (-20 Hz ± 21) Hz for the (±1/2, ±3/2) components. As can be seen, the contribution of the ac Stark shift due to the 1092 nm radiation dominates the systematic shifts. All other contributions are below the 1 Hz (2×10^{-15}) level. When these corrections are applied to the individual runs in the experiment, a corrected value for the 5s $^2S_{1/2}$ – 4d $^2D_{5/2}$ center frequency is obtained:

$$(\nu_{SD})_{corr} = 444\ 779\ 044\ 095\ 510 \pm 50\ \text{Hz}\ (1\sigma) \qquad (24)$$

The corrections bring our result into closer agreement with the measurement of of ν_{SD} = 444 779 044 095 520 ± 100 Hz (1σ) by Margolis et al. [7]. This result strengthens our current knowledge of the Sr^+ ion system, both from the point of view of an improved value for the exact S-D transition frequency, and through a better understanding of the systematic effects, which limit the accuracy. In examining the limitations to the accuracy of the single ion reference frequency, it is clear that the current measurement is limited primarily by the fast, irregular drift rate and spectral profile of the probe laser system. Further improvement in this area will result in an improved value for the ion center frequency. Provided that the systematic shifts can be reduced or calculated, we expect that the ultimate accuracy will be limited by the laboratory's ability to realize the SI second via the available cesium standards.

Concerning the accuracy of the obtained frequency due to the principal systematic limitations of the ion system itself, there are a number of areas where the experiment can be controlled that would yield greatly improved results. Of primary importance will be the isolation of the 1092 nm radiation during the probe interrogation cycle. This will reduce the magnitude of the systematic corrections to the 1 Hz level. Better control of ion micromotion via monitoring in three orthogonal directions [45] could conceivably reduce the second-order Doppler and Stark micromotion contributions to the mHz level. As the resolution of the ion resonance improves, the effects of ac fields on the lineshape could be significantly reduced. The principal systematic shifts remaining are then due to the blackbody radiation shift and the electric quadrupole shift of the D state. The blackbody shift could be effectively removed by cooling the trap apparatus to cryogenic temperatures [46]. Barring such a dramatic and challenging approach, improvements in the ab-initio calculation of the Stark shift parameters would lead to a more exact quantification of the shift. Already, the current calculations indicate that this shift is known to 100 mHz. For the electric quadrupole moment, studies of the shift magnitude by application of a known field gradient would provide experimental determination of the moment. This was in fact demonstrated recently in the Yb^+ system by Schneider et al. [47]. The relative change in quadrupole moment shift with Zeeman component pair can also be used to quantify the quadrupole moment. Also, the magnitude of the shift could be determined by the measurement of the quadrupole shift along three orthogonal quantization directions as proposed by Itano [39]. In closing, it seems quite reasonable to assume that the uncertainties in the systematic shifts can be reduced sufficiently that their contribution to the uncertainty in the Sr^+ S-D transition frequency would be below 10 mHz, thus yielding a potential accuracy of better than 2×10^{-17}.

V. CONCLUSION

We have used an optical frequency comb to measure the $^{88}Sr^+$ S-D center frequency at 445 THz with a standard uncertainty of 50 Hz ($\delta\nu/\nu = 1.1 \times 10^{-13}$). This measurement is in excellent

agreement with a previously reported value and represents an improvement of a factor of 2 in the reported uncertainty. Most of the scatter and uncertainty in the above result is attributable to the linewidth and drift of the probe laser system. A new two-stage cavity-stabilized diode laser system has recently been developed and will be implemented in future work. A detailed study of the systematic shifts for this single ion measurement has been presented and the total estimated uncertainty is currently at the 10 Hz level. The current limitation is by ac Stark shifts from the 1092 nm laser source illuminating the ion during the probe cycle. Suitable shuttering during the probing and cooling sequence can eliminate this perturbation. The remaining perturbations are below 0.5 Hz and can be quantified to better than 0.1 Hz. With further improvements in our knowledge of the ion system and better control of the trap environment, it is likely that the uncertainty in the systematic shifts can be reduced to the 10^{-17} level.

ACKNOWLEDGEMENTS

The authors would like to thank Bruce Warrington (CSIRO) for generously supplying Stark shift and blackbody shift data together with results of his calculations prior to publication. In addition, the authors would like to warmly thank Wayne Itano (NIST) for performing the matrix element calculation for Sr^+ using the Cowan wave function computer code. The important contributions of R. Pelletier and B. Hoger in the construction of the electrical components used in the current experiment are recognized. Finally, the critical contributions of J.S. Boulanger and S. Cundy in the provision of the hydrogen maser reference signal are gratefully acknowledged. This work is been partially supported by contributions from the Canadian Institute for Photonic Innovations (CIPI/ICIP).

References

1. *Proceedings of the Sixth Symposium on Frequency Standards and Metrology*, edited by P. Gill (World Scientific, Singapore, 2002) and references therein.

2. T.J. Quinn, *Metrologia* **40**, 103 (2003).

3. S. Bize, S.A. Diddams, U. Tanaka, C.E. Tanner, W.H. Oskay, R.E. Drullinger, T.E. Parker, T.P. Heavner, S.R. Jefferts, L. Hollberg, W.M. Itano, and J.C. Bergquist, *Phys. Rev. Lett*. **90**, 150802 (2003).

4. Diddams S.A., Udem Th., Bergquist J.C., Curtis E.A., Drullinger R.E., Hollberg L., Itano W.M., Lee W.D., Oates C.W., Vogel K.R., Wineland D.J, *Science*, 2001, **293**, 825-828.

5. A.A. Madej and J.E. Bernard in *Frequency Measurement and Control: Advanced Techniques and Future Trends, Springer Topics in Applied Physics*, Andre N. Luiten editor, vol .**79**, (Springer Verlag, Berlin, Heidelberg, 2001) p. 153 and references therein.

6. J.E. Bernard, A.A. Madej, L. Marmet, B.G. Whitford, K.J. Siemsen, and S. Cundy, *Phys. Rev. Lett.* **82**, 3228 (1999).

7. H.S. Margolis, G. Huang, G.P. Barwood, S.N. Lea, H.A. Klein, W.R.C. Rowley, and P. Gill, Phys. Rev. A **67**, 032501 (2003).

8. J. Stenger, Chr. Tamm, N. Haverkamp, S. Weyers, and H. Telle, *Opt. Lett.* **26**, 1589 (2001).

9. J. v. Zanthier, Th. Becker, M. Eichenseer, A. Yu. Nevsky, Ch. Schwedes, E. Peik, H. Walther, R. Holzwarth, J. Reichert, Th. Udem, T.W. Hänsch, P.V. Pokasov, M.N. Skvortsov, S.N. Bagayev, *Opt. Lett.* **25**, 1729 (2000).

10. Th. Udem, S.A. Diddams, K.R. Vogel, C.W. Oates, E.A. Curtis, W.D. Lee, W.M. Itano, R.E. Drullinger, J.C. Bergquist, and L. Hollberg, *Phys. Rev. Lett*. **86**, 4996 (2001).

11. A.A. Madej and J.D. Sankey, *Opt. Lett.* **15**, 634 (1990).

12. A.A. Madej, L. Marmet, J.E. Bernard, *Appl. Phys. B*, **67**, 229 (1998).

13. G.P. Barwood, P. Gill, H.A. Klein,and W.R.C. Rowley, *IEEE Trans. Instrum. Meas.* **46**, 133 (1997).

14. A.A. Madej , K.J. Siemsen, L. Marmet, J.E. Bernard, and O. Acef, , *IEEE Trans. Instrum. Meas.,* **48** , 553 (1999).

15. G. Barwood, K. Gao, P. Gill, G. Huang, H.A. Klein, *IEEE Trans. Instrum. Meas.* **50**, 543 (2001).

16. J.E. Bernard, A.A. Madej, P. Dubé, L. Marmet, A. Czajkowski, and R.S. Windeler, in *Proceedings of the 2003 IEEE International Frequency Control Symposium Jointly with the 17th European Frequency and Time Forum*, John R. Vig editor (IEEE Press, Piscataway NJ, USA, 2003) IEEE Catalog No. 03CH37409, p. 162.

17. J.E. Bernard, L. Marmet, and A.A. Madej, *Optics Comm.*, **150**, 170 (1998).

18. L. Marmet, A.A. Madej, K.J. Siemsen, J.E. Bernard, and B.G. Whitford, *IEEE Trans. Instrum. Meas.* **46**, 169 (1997).

19. J.D. Sankey and A.A. Madej, *Appl. Phys. B* **49**, 69 (1989).

20. P. Dubé, L. Marmet, J.E. Bernard, K.J. Siemsen, and A.A. Madej in *Proceedings of the Sixth Symposium on Frequency Standards and Metrology*, edited by P. Gill (World Scientific, Singapore, 2002) pp.489-491.

21. T. Udem , J. Reichert, R. Holzwarth ,and T.W. Hänsch, *Phys. Rev. Lett.*, **82**, 3568 (1999).

22. D.J Jones, S.A. Diddams, J.K. Ranka, R.S.Windeler, A.J. Stentz, J.L. Hall, and S.T. Cundiff, *Science*, **288**, 635 (2000).

23. S.A. Diddams, Th. Udem, K.R. Vogel, C.W. Oates, E.A. Curtis, R.S. Windeler, A. Bartels, J.C. Berquist, and L. Holberg, "A compact femtosecond-laser-based optical clockwork", in *Laser Frequency Stabilization, Standards, Measurement, and Applications*, John L. Hall, Jun Ye, Editors, Proceedings of SPIE Vol. **4269**, (SPIE, Bellingham, WA, 2001), pp.77-83.

24. A.A. Madej, J.E. Bernard, L. Robertsson, L.-S. Ma, M. Zucco, and R.S. Windeler, "Long Term Absolute Frequency Measurements of 633 nm Iodine Stabilized Laser Standards at NRC and Demonstration of High Reproducibility of such Devices in International Frequency Measurements", *Metrologia* (submitted for publication, 2003).

25. J.K. Ranka, R.S. Windeler, and A.J. Stentz., *Opt. Lett.* **25**, 25 (2000).

26. S. Urabe, M. Watanabe, H. Imajo, K. Hayasaka, U. Tanaka, and R. Ohmukai, *Appl. Phys. B* **67**, 223 (1998).

27. D.J. Berkeland, J.D. Miller, J.C. Bergquist, W.M. Itano, and D.J. Wineland, *J. Appl. Phys.* **83**, 5025 (1998).

28. A. Khadjavi, A. Lurio, and W. Happer, *Phys. Rev.* **167**, 128 (1968).

29. A. Gallagher, *Phys. Rev.* **157**, 24 (1967).

30. T. Brage, G.M. Wahlgren, S.G. Johansson, D.S. Leckone, and C.R. Proffitt, *Astrophys. J.* **496**, 1051 (1998).

31. W.L. Wiese, M. W. Smith, and B.M. Miles, *Nat. Stand. Ref. Data Ser. Nat. Bur. Stand. (U.S.)* **22**, Vol. II, (U.S. Gov't Printing Office, Washington D.C.) (1969).

32. B. Warrington, private communication (2003).

33. J.R.P. Angel and P.G.H. Sandars, *Proc. Roy. Soc. A* **305**, 125 (1968).

34. J.W. Farley and W.H. Wing, *Phys. Rev. A* **23**, 2397 (1981).

35. W.M. Itano, L.L. Lewis, and D.J. Wineland, *Phys. Rev. A* **23**, 1233 (1982).

36. A. Bauch and R. Schröde, *Phys. Rev. Lett.* **78**, 622 (1997).

37. I.I. Sobel'man, *Introduction to the Theory of Atomic Spectra* (Pergamon, Oxford, 1972), p. 275.

38. L. Marmet and A.A. Madej, *Can. J. Phys.* **78**, 495 (2000).

39. W. M. Itano, *J. Res. Nat. Inst. Stand. Technol.* **105**, 829 (2000).

40. E.E. Anderson, *Modern Physics and Quantum Mechanics,* (W.B. Saunders Co., Philadelphia, PA, 1971) p.288.

41. W.M. Itano, private communication.

42. R.D. Cowan, *The Theory of Atomic Structure and Spectra*, (Univ. California Press, Berkeley, 1981).

43. T. Su and M.T. Bowers, in *Gas Phase Ion Chemistry*, edited by M.T. Bowers (Academic, New York, 1979), Vol. 1, p.83.

44. B.P. Stoicheff and E. Weinberger, *Phys. Rev. Lett.* **44**, 733 (1980).

45. A.G. Sinclair, M.A. Wilson, and P. Gill, *Opt. Commun.* **190**, 193 (2001).

46. M.E. Poitzsch, J.C. Bergquist, W.M. Itano, and D.J. Wineland, *Rev. Sci. Instrum.* **67**, 129 (1996).

47. T. Schneider, Chr. Tamm, E. Peik, in *Proceedings of the 2003 IEEE International Frequency Control Symposium Jointly with the 17th European Frequency and Time Forum*, John R. Vig editor (IEEE Press, Piscataway NJ, USA , 2003) IEEE Catalog No. 03CH37409, p. 162.

List of Table Captions

TABLE I: Compilation of oscillator strengths used for the calculation of Stark shift coefficients for the 445-THz 5s $^2S_{1/2}$ –4d $^2D_{5/2}$ transition in $^{88}Sr^+$. Reference data include the calculated oscillator strengths of Brage et al. [30], scaled oscillator strengths of Ca^+ from reference [31], and experimental values obtained from Gallagher [29].

TABLE II: Calculated ac Stark shift coefficients for the 5s $^2S_{1/2}$ and 4d $^2D_{5/2}$ levels using incident radiation at 674 nm resonant with the 5s $^2S_{1/2}$ –4d $^2D_{5/2}$ transition. The calculations are performed using the oscillator strength data sets given in Table I.

TABLE III: Calculated ac Stark shift coefficients for the 5s $^2S_{1/2}$ and 4d $^2D_{5/2}$ levels using incident radiation at 1092 nm resonant with the 4d $^2D_{3/2}$- 5p $^2P_{1/2}$ transition. The calculations are performed using the oscillator strength data sets given in Table I.

TABLE IV: Summary of determined frequency systematic shifts and their estimated uncertainty for the current series of experimental measurements.

Transition	Wavelength (nm)	f		
		Brage et al. Ref.[30]	Scaled Ca^+ Ref.[31]	Gallagher Ref.[29]
$5s\ ^2S_{1/2} - 5p\ ^2P_{1/2}$	421.67	0.334	0.3383	0.34 ± 0.015
$5s\ ^2S_{1/2} - 5p\ ^2P_{3/2}$	407.89	0.693	0.7080	0.71 ± 0.03
$4d\ ^2D_{5/2} - 5p\ ^2P_{3/2}$	1033	0.076	0.096	0.096 ± 0.02
$4d\ ^2D_{5/2} - 6p\ ^2P_{3/2}$	242.6		0.0015	
$4d\ ^2D_{5/2} - 7p\ ^2P_{3/2}$	185.3		0.0006	
$4d\ ^2D_{5/2} - 4f\ ^2F_{5/2}$	216.7	0.012	0.016	
$4d\ ^2D_{5/2} - 5f\ ^2F_{5/2}$	177.8		0.0074	
$4d\ ^2D_{5/2} - 6f\ ^2F_{5/2}$	162.0		0.004	
$4d\ ^2D_{5/2} - 7f\ ^2F_{5/2}$	153.8		0.002	
$4d\ ^2D_{5/2} - 8f\ ^2F_{5/2}$	148.9		0.0016	
$4d\ ^2D_{5/2} - 4f\ ^2F_{7/2}$	216.7	0.238	0.317	
$4d\ ^2D_{5/2} - 5f\ ^2F_{7/2}$	177.8		0.148	
$4d\ ^2D_{5/2} - 6f\ ^2F_{7/2}$	162.0		0.079	
$4d\ ^2D_{5/2} - 7f\ ^2F_{7/2}$	153.8		0.048	
$4d\ ^2D_{5/2} - 8f\ ^2F_{7/2}$	148.9		0.031	

Table I

Energy Level	κ (mHz/(W/m^2))		
	Brage et al. Ref. [30]	Gallagher Ref. [29]	Scaled Ca^+ Ref. [31]
5s $^2S_{1/2}$	-0.631	-0.645	
4d $^2D_{5/2}$ (m = ±1/2)	+0.055		+0.047
4d $^2D_{5/2}$ (m = ±3/2)	+0.094		+0.095
4d $^2D_{5/2}$ (m = ±5/2)	+0.17		+0.19

Table II

Energy Level	κ (mHz/(W/m^2))		
	Brage et al. Ref. [30]	Gallagher Ref. [29]	Scaled Ca^+ Ref. [31]
5s $^2S_{1/2}$	-0.460	-0.470	
4d $^2D_{5/2}$ (m = ±1/2)	-1.1		-1.4
4d $^2D_{5/2}$ (m = ±3/2)	-1.6		-2.0
4d $^2D_{5/2}$ (m = ±5/2)	-2.7		-3.4

Table III

Source of Systematic Shift	Shift of Line Center [Hz]	Uncertainty of shift [Hz]	Fractional Magnitude of Shift
Thermal Contribution to Second Order Doppler Effect	-0.027	0.007	6×10^{-17}
Micromotion Contribution to Second Order Doppler Effect	-0.16	0.10	4×10^{-16}
Blackbody ac Stark Shift	+0.30	0.11	7×10^{-16}
Thermal Contribution to Stark shift	+0.036 (±1/2,±1/2) +0.029 (±1/2,±3/2)	0.018 0.012	8×10^{-17} 7×10^{-17}
Micromotion Contribution to Stark Shift	+ 0.9 (±1/2, ±1/2) + 0.7 (±1/2, ±3/2)	0.9 0.7	2×10^{-15}
Ac Stark Shift due to 674nm light	+0.10 (±1/2, ±1/2) +0.10 (±1/2, ±3/2)	0.06 0.06	2×10^{-16}
Ac Stark Shift due to 1092nm light	-12 (±1/2, ±1/2) -21 (±1/2, ±3/2)	12 21	3×10^{-14} 5×10^{-14}
Electric Quadrupole Shift of the 4d $^2D_{5/2}$ level	< 0.55 (±1/2, ±1/2) < 0.14 (±1/2, ±3/2)	0.55 0.14	1×10^{-15} 3×10^{-16}
Ac field shift via linear Zeeman effect	< 0.2 (±1/2, ±1/2) < 0.4 (±1/2, ±3/2)	0.2 0.4	4×10^{-16} 9×10^{-16}
Quadratic Zeeman effect due to bias field	+0.0011 (±1/2, ±1/2) +0.00040 (±1/2, ±3/2)	0.0002 0.00006	2×10^{-18} 9×10^{-19}
Blackbody contribution to Quadratic Zeeman shift	$+ 4.0 \times 10^{-5}$ (±1/2, ±1/2) $+ 2.6 \times 10^{-5}$ (±1/2, ±3/2)		9×10^{-20} 6×10^{-20}
Collisional Shift	< 0.005	0.005	1×10^{-17}
Estimated Total Systematic Shifts	-10 (±1/2, ±1/2) -20 (±1/2, ±3/2)	12 21	3×10^{-14} 5×10^{-14}

Table IV

List of Figure Captions

Figure 1: Partial energy level Diagram of $^{88}Sr^{+}$ showing the principal transitions used in cooling, fluorescence detection, repumping, and probing of the reference 445 THz (674nm) transition.

Figure 2: Schematic diagram of the NRC femtosecond laser frequency comb system.

Figure 3: Spectrum of the ($m_{J''}$, $m_{J'}$) = (-1/2, -1/2) Zeeman component of the S-D transition showing the general signal level and linewidth used in the current series of measurements. The error bars are calculated from the number of quantum jumps assuming Poisson counting statistics. The fitted curve is of Lorentzian form and yields a linewidth of (410 ± 50) Hz.

Figure 4: Plot of the observed linewidth of the S-D Zeeman components as a function of the relative distance from line center. The plot shows that there is no variation in linewidth within experimental uncertainty.

Figure 5: Example of experimental run data obtained in the determination of the $^{88}Sr^{+}$ S-D center frequency. a) Series of 1s absolute frequency determinations of the 445-THz probe laser used to interrogate the ion transition. b) Series of 20s determinations of the AOM shift frequency needed to maintain the 445-THz fixed probe laser into resonance with the center of the single ion transition. c) Final combined determination of the center S-D frequency.

Figure 6: The Allan standard deviation from the 1s readings of the absolute probe laser as measured with the NRC frequency comb system (solid circles). Also shown is the Allan deviation for successive 20 s determinations of the center S-D frequency (open triangles).

Figure 7: Summary of all absolute frequency determinations of center S-D frequency taken over a four month period spanning August 2002 – November 2002 comprising the different four experimental day runs. The solid line corresponds to the weighted mean of all the frequency values.

Figure 8: Plot of the relative position of the S-D line center as a function of the applied axial trim differential voltage applied to the endcap electrodes of the Paul trap. The voltage yielding minimum micromotion during these experiments was V_{ax} = -0.6 V.

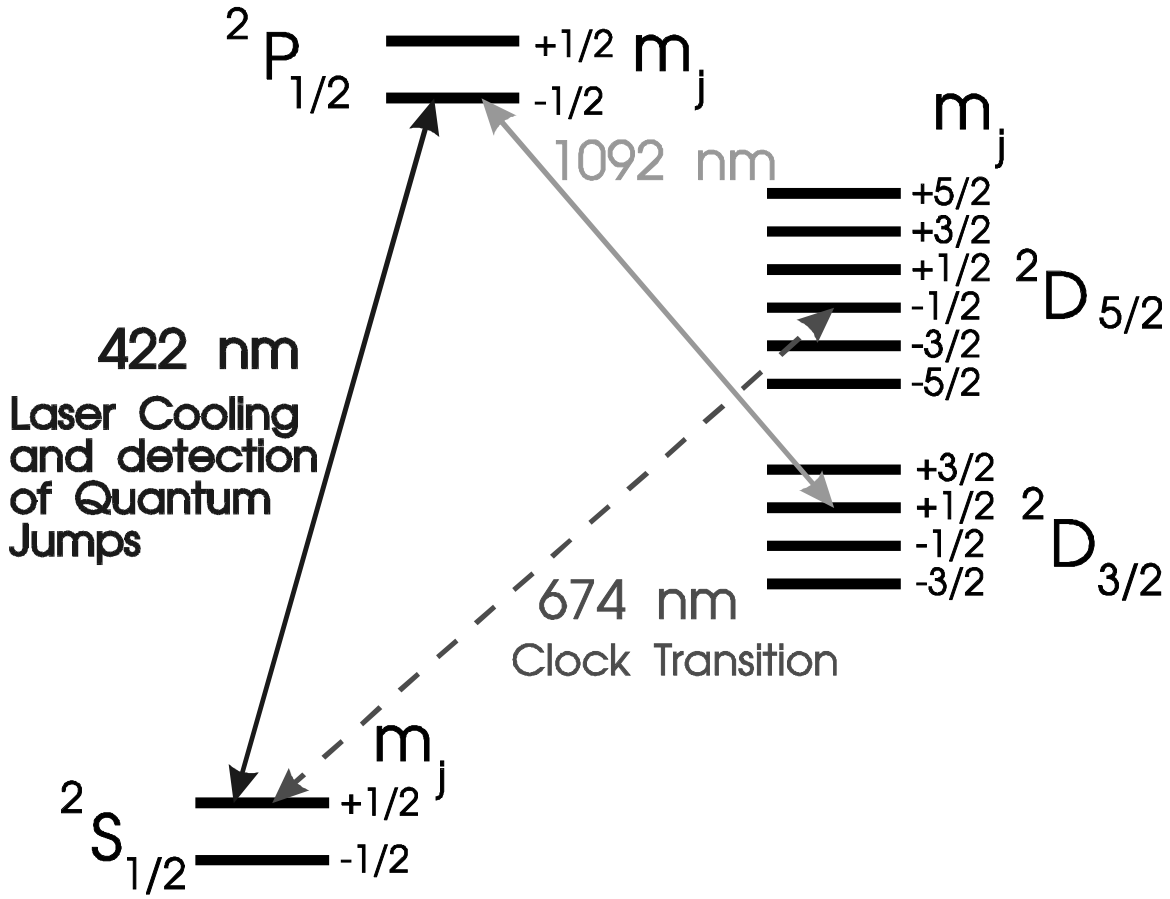
$^2P_{1/2}$
+1/2
-1/2
m_j
1092 nm
m_j
+5/2
+3/2
+1/2
-1/2
-3/2
-5/2
$^2D_{5/2}$
422 nm
Laser Cooling
and detection
of Quantum
Jumps
+3/2
+1/2
-1/2
-3/2
$^2D_{3/2}$
674 nm
Clock Transition
m_j
$^2S_{1/2}$
+1/2
-1/2

Figure 1

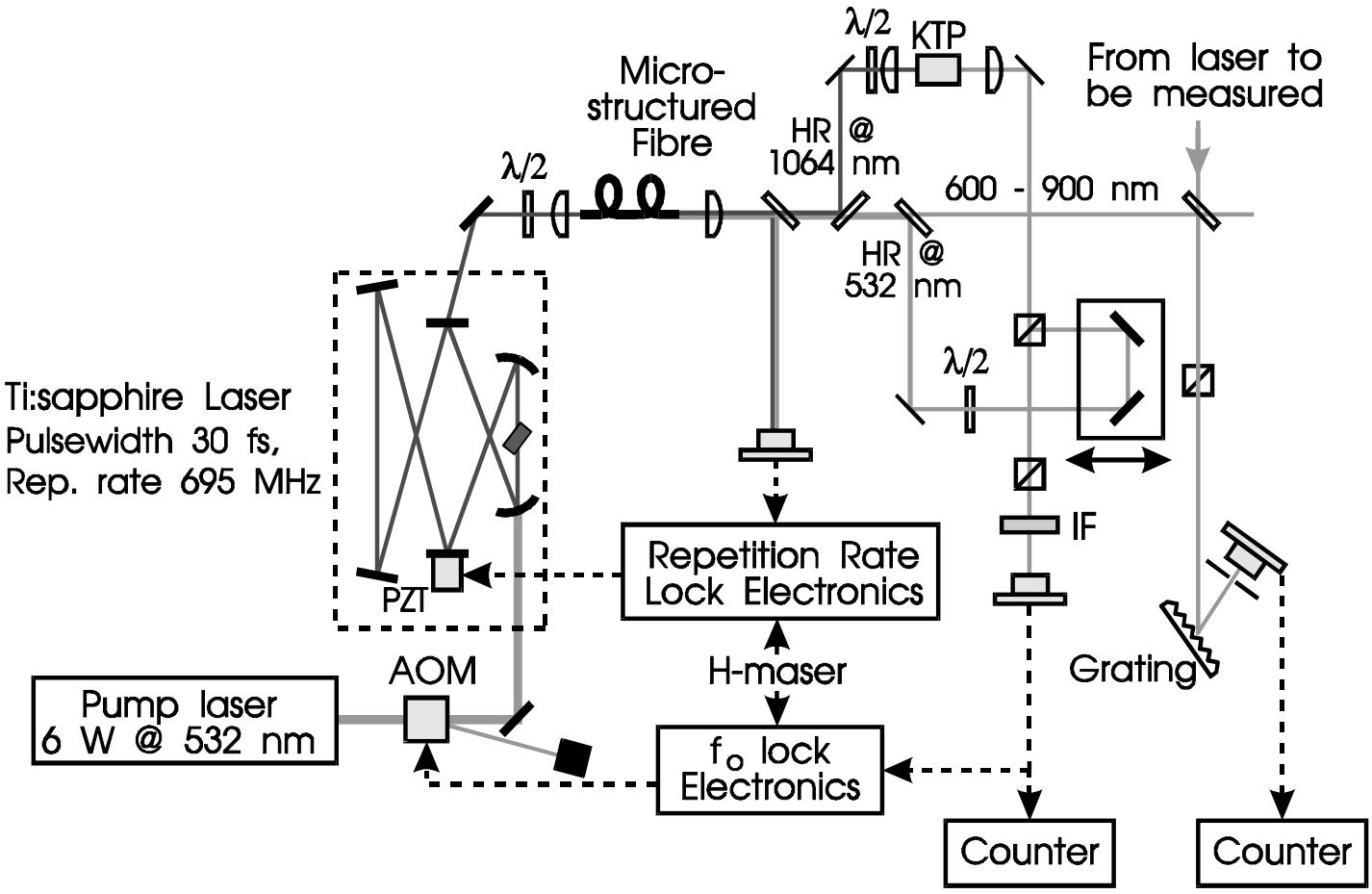
λ/2
KTP
From laser to be measured
Micro-structured Fibre
HR @ 1064 nm
λ/2
600 - 900 nm
HR @ 532 nm
λ/2
Ti:sapphire Laser
Pulsewidth 30 fs,
Rep. rate 695 MHz
IF
Repetition Rate Lock Electronics
PZT
AOM
H-maser
Grating
Pump laser 6 W @ 532 nm
f_o lock Electronics
Counter
Counter

Figure 2

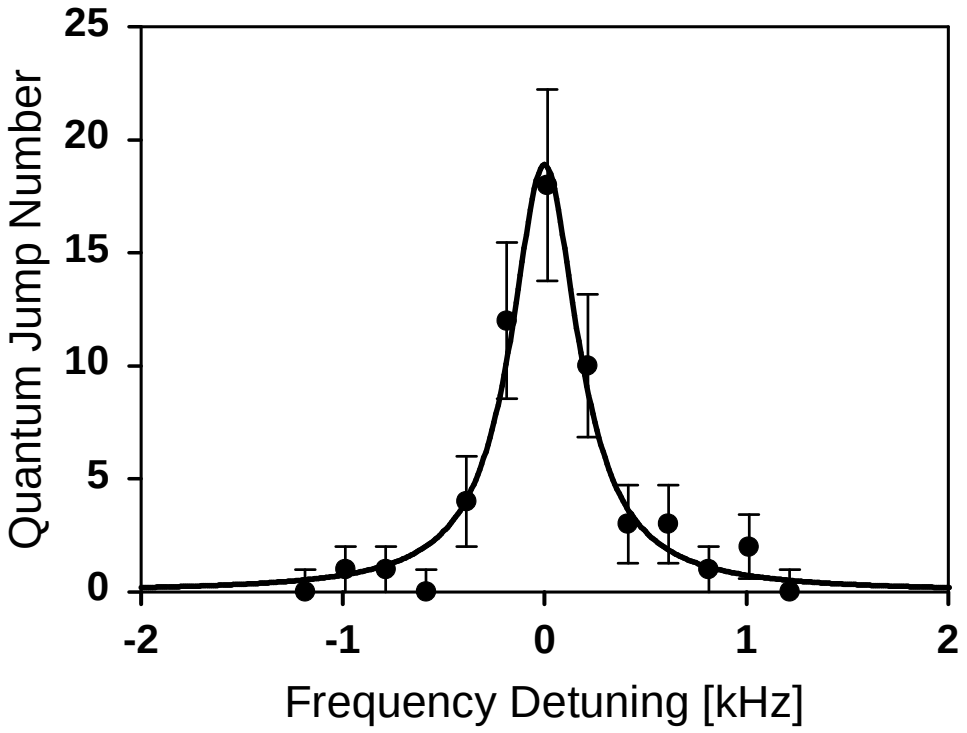
Quantum Jump Number
25
20
15
10
5
0
-2
-1
0
1
2
Frequency Detuning [kHz]

Figure 3


Component Linewidth [Hz]
500
450
400
350
0
1
2
3
4
5
6
Relative Zeeman Shift

Figure 4

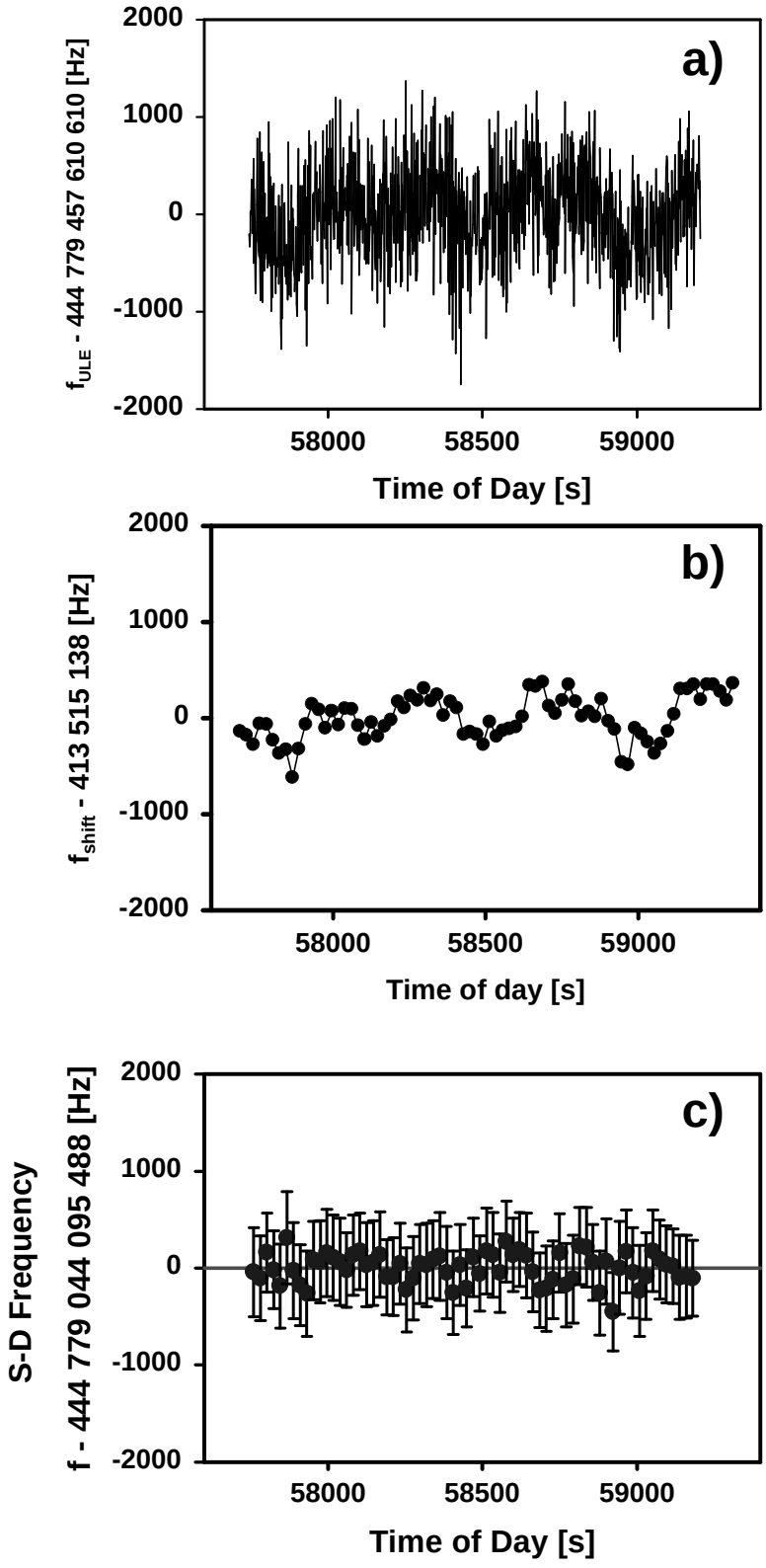
a)
2000
1000
0
-1000
-2000
f_{ULE} - 444 779 457 610 610 [Hz]
58000
58500
59000
Time of Day [s]
b)
2000
1000
0
-1000
-2000
f_{shift} - 413 515 138 [Hz]
58000
58500
59000
Time of day [s]
c)
2000
1000
0
-1000
-2000
S-D Frequency
f - 444 779 044 095 488 [Hz]
58000
58500
59000
Time of Day [s]

Figure 5

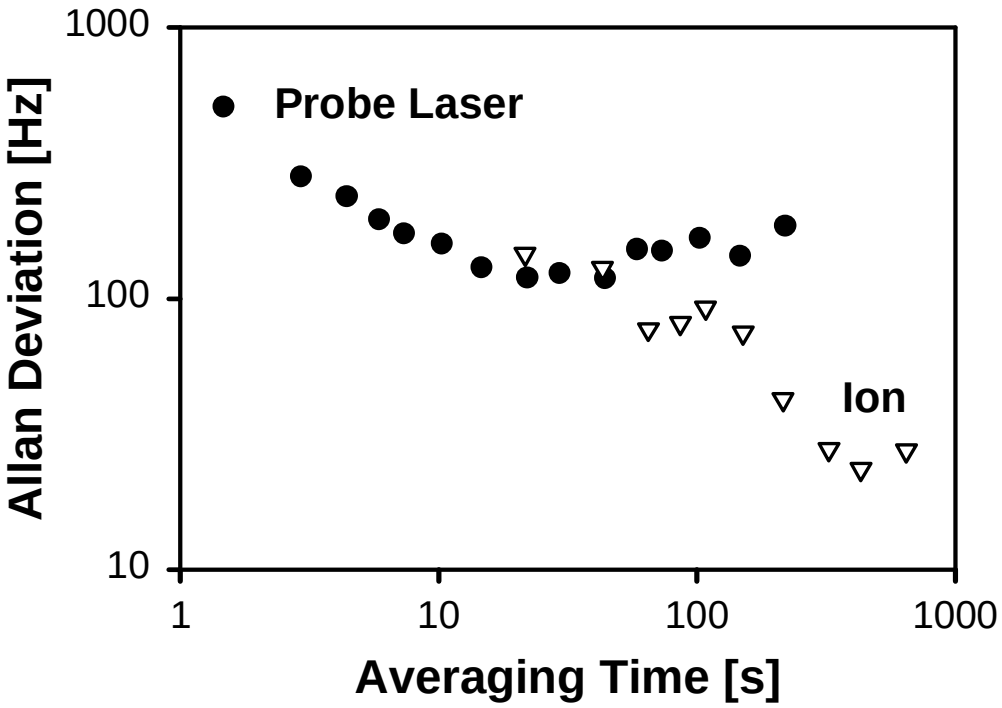
1000
100
10
Allan Deviation [Hz]
Probe Laser
Ion
1
10
100
1000
Averaging Time [s]

Figure 6

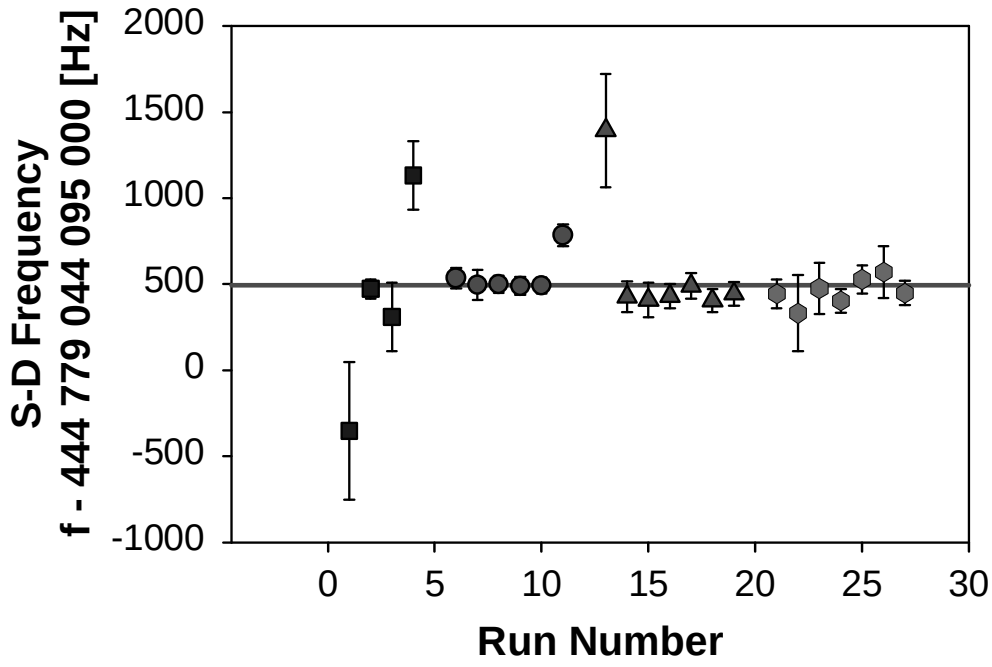
S-D Frequency
f - 444 779 044 095 000 [Hz]
2000
1500
1000
500
0
-500
-1000
0
5
10
15
20
25
30
Run Number

Figure 7

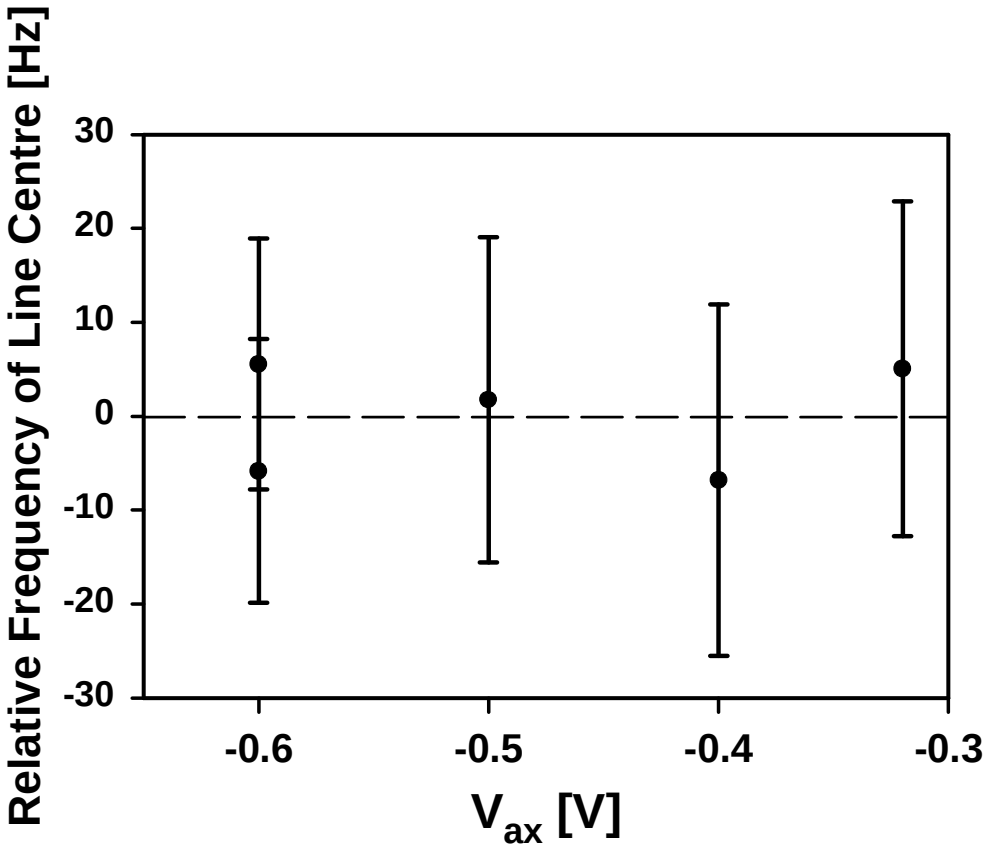
Relative Frequency of Line Centre [Hz]
30
20
10
0
-10
-20
-30
-0.6
-0.5
-0.4
-0.3
V_{ax} [V]

Figure 8